Available online at www.sciencedirect.com

SciVerse ScienceDirect

Ceramics International 39 (2013) 3873–3879

CERAMICS INTERNATIONAL

www.elsevier.com/locate/ceramint

Synthesis and electrical properties of co-doping with La^{3+}, Nd^{3+}, Y^{3+}, and Eu^{3+} citric acid-nitrate prepared samarium-doped ceria ceramics

Massoud Kahlaoui*, Sami Chefi, Abdelwahab Inoubli, Adel Madani, Chaabane Chefi

Laboratoire de physique des matériaux, Faculté des Sciences de Bizerte, Université de Cartage, Zarzouna 7021, Tunisia

Received 6 September 2012; received in revised form 9 October 2012; accepted 19 October 2012
Available online 8 November 2012

Abstract

Fluorite oxides $Ce_{0.8}Sm_{0.1}Ln_{0.1}O_{1.9}$ (denoted as SDC for singular doping and LnSDC for Ln = La, Nd, Y and Eu), were prepared by the citric acid–nitrate combustion reaction to act as electrolytes for intermediate-temperature solid oxide fuel cells (IT-SOFC). The thermal decomposition, phase identification, morphology, density, particle size distribution and electrical properties of the samples were studied by TGA/TDA, XRD, SEM, the Archimedes method, a laser size analyzer and Impedance spectroscopy, respectively. All crystallite powders that calcined at 800 °C had a cubic fluorite structure; the average crystallite size was between 63 and 68.5 nm. The pellets were then sintered at 1400 °C in air for 7 h. The relative densities of these pellets were over 95%, which was in good agreement with the results of the SEM. The impedance measurements were performed in an open circuit using two electrode configurations. The results showed that $Ce_{0.8}Sm_{0.1}La_{0.1}O_{1.9}$ had the highest electrical conductivity, $\sigma_{700\,^{\circ}C}$, equal to 6.59×10^{-2} S cm^{-1} and the lowest activation energy equal to 0.85 eV. It was therefore concluded that co-doping with the appropriate rare-earth cations can further improve the electrical properties of ceria electrolytes.

Keywords: C. Ionic conductivity; SOFC; Citric acid-nitrate process; Co-doping

1. Introduction

Doped ceria oxides are usually considered a good ionic electrolyte at intermediate temperatures for solid oxide fuel cells (IT-SOFC), whose electronic conductivity is negligible at moderate temperatures (< 800 °C) in the absence of a reducing atmosphere. Among the doped ceria-based solid electrolytes showing high ionic conductivity were: the yttria-doped ceria (YDC), the gadolinia-doped ceria (GDC), the samaria-doped ceria (SDC) and others [1–8]. The electrical and structural properties of doped ceria are influenced by several factors which have been the subject of many studies [9–11]. However, the factors affecting the conduction properties of this solid electrolyte are very complex. Said properties can be strongly influenced by the type and the amount of dopant and by the use synthesis method. So far, some co-doped ceria-based electrolytes have been studied, such as $Ce_{0.8}Gd_{0.15}M_{0.05}O_{2\delta}$, $Ce_{0.8}Gd_{0.18}M_{0.02}O_{2-\delta}$ (for M: Sm Bi, La, and Nd) [12,13], $Ce_{1-x}(Sm_{0.5}Nd_{0.5})_xO_\delta$ [14], $Ce_{0.8}Gd_{0.2-x}Nd_xO_{2-\delta}$ [15], $(Ce_{0.84}Y_{0.16}O_{1.92})_{1-x}(ZnO)_x$ [16], $Ce_{0.8}Y_{0.2-x}Sr_xO_{2-\delta}$ [17], $Ce_{0.8}Gd_{0.2-x}Y_xO_{2-\delta}$ [18] and $Ce_{0.8-x}Sm_{0.2}Ca_xO_{2-\delta}$ [19]. Results have showed that the co-doping method was effective in improving the electrical properties of the ceria-based electrolyte. In previous studies [9,14,15] it was shown that there is a critical doping level (between 10% and 20%) beyond which a high temperature treatment leads to the appearance of micro-domains. It was also shown that the doping elements Sm^{3+}, Y^{3+}, La^{3+}, Nd^{3+}, and Eu^{3+} tend to form large clusters with oxygen vacancies.

In the present study, the composition $Ce_{0.8}Sm_{0.1}Ln_{0.1}O_{1.9}$, denoted as LnSDC ($Ln^{3+} = Y^{3+}$, La^{3+}, Nd^{3+}, Eu^{3+}), was prepared by using the citric acid–nitrate combustion method. The effect of the co-doping element on the structural properties and on the ionic conductivity

*Corresponding author. Tel.: +216 72591906; fax: +216 72590566.
E-mail address: kahlaouimessaoud@yahoo.fr (M. Kahlaoui).

0272-8842/$ - see front matter © 2012 Elsevier Ltd and Techna Group S.r.l. All rights reserved.
http://dx.doi.org/10.1016/j.ceramint.2012.10.230

was compared to singly-doped ceria. The aim was to develop new ceria-based electrolyte materials to further improve the ionic conductivity.

2. Experimental

2.1. Sample preparation

$Ce_{0.8}Sm_{0.1}Ln_{0.1}O_{1.9}$ electrolytes (Ln = La, Nd, Y, Eu) were synthesized using the citric acid–nitrate combustion method. All starting materials used were highly pure: cerium (III) nitrate hexahydrate $Ce(NO_3)_3 \cdot 6H_2O$, 99.99 % (Aldrich), samarium oxide (Sm_2O_3), 99.99 % (Aldrich), lanthanum oxide (La_2O_3), 99.99 % (Aldrich), neodymium oxide (Nd_2O_3), 99.99 % (Aldrich), yttrium oxide (Y_2O_3), 99.99 % (Aldrich), and europium oxide (Eu_2O_3), 99.99 % (Aldrich). Cerium nitrate was dissolved in distilled water and the corresponding amount of samaria and (Ln_2O_3) oxide was dissolved in a nitrate solution. The individual solutions were then mixed together in a glass beaker. Aqueous solutions of citric acid and ammonium nitrate were then added to the mixture mentioned above (the mole ratio of cation to citric acid was 1:1.3 and pH = 7.2). A white gel was obtained after continuous stirring at 85 °C for 7–11 h depending on the Ln-doping element. The gel was then dried and placed in a sand bath; bubbles formed and the resulting solid swelled to produce a rigid foam of glassy appearance. The final step, the self-burning of the foam, took place spontaneously and led to the formation of an airy meringue-like substance. After being crushed in an agate mortar and after releasing the nitrate through heat treatment, the sample was sintered in air at 800 °C for 5 h in order to obtain the desired compound, which was proved to be pure by X-ray characterization. It should be noted that the oxidation of Ce^{3+} to Ce^{4+} occurs during this stage [10].

2.2. Structural characterization

Before calcinations, the SDC was studied by means of the (TGA/TDA) thermogravimetric and differential analyses, using the TG–DTA 92 SETARAM equipment in flowing air, in a temperature ranging from room temperature to 800 °C at a heating rate of 5 °C/min. The composition phase of the obtained LnSDC powders was identified by X-ray diffraction (XRD) with a Brukers D8 Advance Germany diffractometer which uses Cukα monochromatic radiation at room temperature. The crystalline phase and cell parameters were fitted with the PANalytical X'Pert High Score Plus program using the Rietveld method. The average crystallite size (D) was also defined by using the Scherrer formula [20]: $D = 0.9\lambda/\beta\cos\theta$. The morphology and microstructure of LnSDC powders were observed with a scanning electron microscope (SEM), JEOL.JSM-5400. A laser size analyzer (Malvern Mastersizer 2000) was used to measure the particle size distribution. The dried powders were grinded in an agate mortar and then pressed at 5 MPa into cylindrical pellets (12–13 mm in diameter and 0.8–1.5 mm in thickness). Following the density results found by Karaca et al. [2], pellets were sintered at 1400 °C in air for 7 h with a heating and cooling rate of 200 °C/h. The density of the sintered pellets was determined through the Archimedes method and was then compared to the theoretical values determined by the lattice parameters.

2.3. Electrical measurements

Electrochemical Impedance Spectra (EIS) were obtained using a Hewlett-Packard HP 4192 analyzer. The impedance measurements were taken in an open circuit using two electrode configurations with signal amplitude of 50 mV and a frequency band ranging from 5 Hz to 13 MHz. Both pellet surfaces were coated with silver pastes electrodes while the platinum wires attached to the electrodes were used as current collectors. All these measurements were performed at equilibrium potential at a temperature ranging between 300 and 700 °C. In order to obtain the bulk, grain boundary and total ionic conductivities, the resulting data was analyzed using the equivalent circuit of the Zview software.

3. Results and discussion

3.1. Thermal analysis

Fig.1 shows the simultaneous TGA/DTA curves of the dried $Ce_{0.8}Sm_{0.2}O_{1.9}$ (SDC) foam. In the DTA curve, two of the endothermic peaks, those around 95 °C and 225 °C, can be attributed to the dehydration and the initial thermal decomposition of the dried foam respectively. The two pronounced exothermic peaks around 300 °C and 450 °C probably correspond to the burning of the residual organic matter and to the gradual crystallization of SDC. As the TGA curve shows, the sample gradually loses weight below 450 °C. The first weight loss occurs between 50 and 100 °C; the second abrupt loss weight is observed between 250 and 400 °C. No remarkable change can be seen above 550 °C in

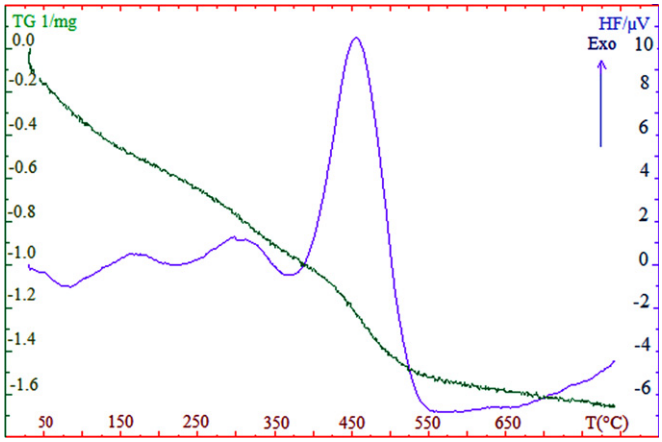

Fig. 1. TG–DTA curves of the thermal decomposition of SDC powder precursors at a heating rate of 5 °C min^{-1} in static air.

the TGA/DTA curves. This proves that LnSDC has been almost perfectly crystallized beyond this temperature.

3.2. Crystal structure

Fig. 2(a) shows the XRD patterns of the $Ce_{0.8}Sm_{0.1}Ln_{0.1}O_{1.9}$ (LnSDC) solid solutions which were prepared by an acid combustion process and calcined at 800 °C for 5 h. It can be clearly seen that all powders were single-phased with a cubic fluorite structure and space group Fm3m (JCPDS powder diffraction file no. 34-0394). No other peaks attributed to impurities or other phases were detected.

The crystallite sizes (D_{XRD}) of the LnSDC powders, calculated by the Scherrer formula, were found to be between 63 and 68.5 nm (Table 1). The co-doping of rare-earth oxides into CeO_2 can cause a small shift in the ceria peaks (Fig. 2(b)); this suggests a change in lattice parameters.

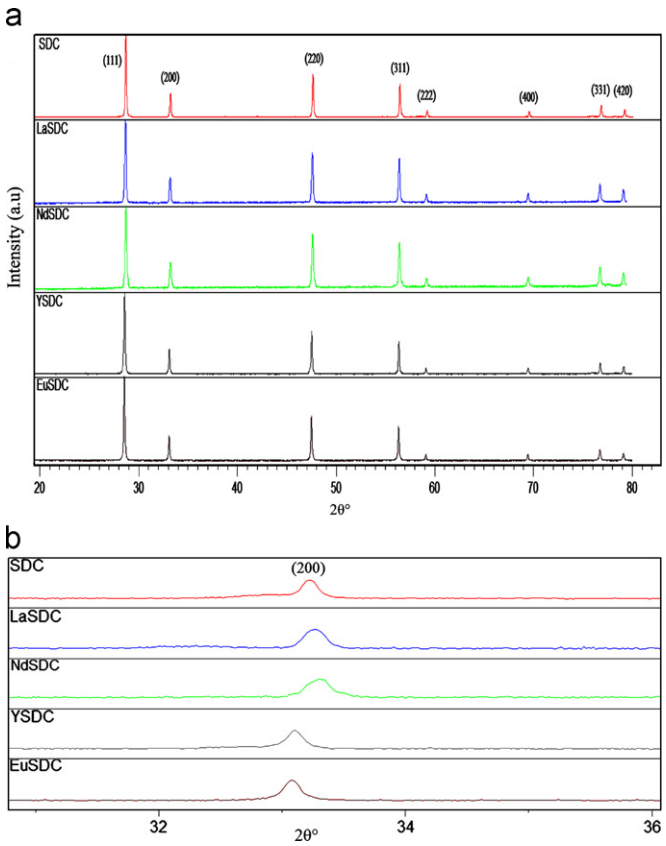

Fig. 2. (a) Powder X-ray diffraction patterns of $Ce_{0.8}Sm_{0.1}Ln_{0.1}O_{1.9}$ (Ln=La, Nd, Y, Eu) solid solutions. (b) Shift in (200) XRD peak position of $Ce_{0.8}Sm_{0.1}Ln_{0.1}O_{1.9}$ with different Ln cations.

During the formation of LnSDC solid solutions, the defect reaction is described by the following formula proposed by Mogensen et al. [9]:

$$2CeO_2 \xrightarrow{2MO_{1.5}} 2M'_{Ce} + V_O + 3^x_O \quad (1)$$

The theoretical lattice parameters, a_c (r_M), for all LnSDC solid solutions are given by the following formula:

$$a_c(r_M) = \frac{4}{\sqrt{3}}\left[0.2r_M + 0.8r_{Ce} + 0.95r_O + 0.05r_{V_O}\right] \times 0.99971 \quad (2)$$

where r_{Ln}, r_{Ce}, r_O and r_{V_O} are the Ln, Ce, O and oxygen vacancy radii respectively. For M=Sm+Ln, r_M is the average ion radius of $Sm^{3+}+Ln^{3+}$.

As shown in Table 1, the measured unit cell parameters, a_m, for LnSDC are greater than the fluorite SDC lattice constant (5.406 Å), which indicates that introducing Ln^{3+} into SDC can cause swelling of the crystal lattice. Co-doping samarium-doped ceria ceramics with La^{3+}, Nd^{3+}, Y^{3+}, and Eu^{3+} causes elastic deformation of the material and thus shows a uniform strain in the lattice causing the diffraction peaks to shift to new 2θ positions (Fig. 2(b)). Similar results had been reported by Fu et al. [20] for $Ce_{0.8}M_{0.2}O_{1.9}$ ceramics prepared by the co-precipitation method for M=Y, Gd, Sm, Nd, and La. As seen in Fig. 3 the measured lattice parameters are in accordance with the calculated parameters, proving that the defect reaction is reasonable.

3.3. Microstructure

The calculated density (D_c), the measured sintered density (D_m) and the relative density (D_m/D_c) are summarized in Table 1. However, the measured density of all samples is greater than the theoretical value by 95%, while ceria solid electrolytes prepared by conventional ceramic processing techniques require over 1500 °C and 1600 °C respectively in order to obtain this density [9,21].

The sintered density of all samples was determined using the equation of the Archimedes principle:

$$D_m = \frac{M_0\,\rho_{water}}{M_1 - M_2} \quad (3)$$

where M_0 is the mass of dry samples, M_1 is the wet mass (water in body), M_2 is the body's submerged mass and ρ_{water} is the density of water at the mass temperatures.

Table 1
Measured and calculated properties of the $Ce_{0.8}Sm_{0.1}Ln_{0.1}O_{1.9}$ series.

Composition	D_{XRD} (nm)	S	a_c (Å)	a_m (Å)	D_c (g cm^{-3})	D_m(g cm^{-3})	D_m/D_c (%)
$Ce_{0.8}Sm_{0.2}O_{1.9}$	66.8	1.97	5.437	5.406	7.13	6.78	95.2
$Ce_{0.8}Sm_{0.1}La_{0.1}O_{1.9}$	63.6	2.99	5.453	5.447	7.02	6.76	96.4
$Ce_{0.8}Sm_{0.1}Nd_{0.1}O_{1.9}$	64.1	2.69	5.444	5.441	7.07	6.79	96.1
$Ce_{0.8}Sm_{0.1}Y_{0.1}O_{1.9}$	68.5	2.60	5.425	5.413	6.92	6.62	95.7
$Ce_{0.8}Sm_{0.1}Eu_{0.1}O_{1.9}$	65.4	2.52	5.434	5.415	7.15	6.90	96.6

The equation used for calculating the theoretical density (D_c) is as follows [20]:

$$D_c = \frac{0.8M_d + 3.2M_{Ce} + 7.6M_O}{N_A[a_c]^3} \quad (4)$$

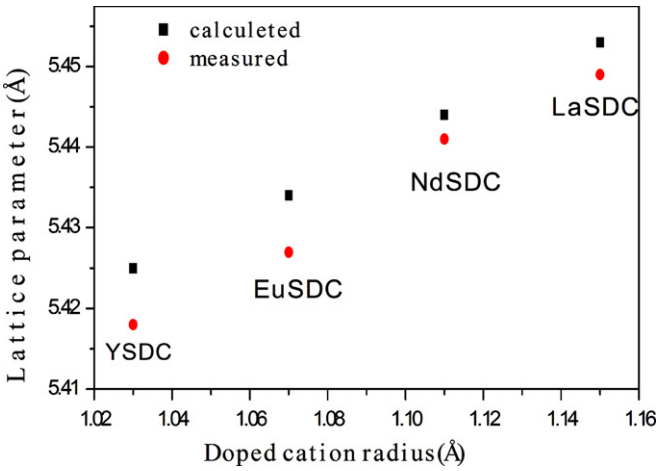

Fig. 3. Calculated and measured lattice parameters of $Ce_{0.8}Sm_{0.1}Ln_{0.1}O_{1.9}$ (Ln = La, Nd, Y, Eu) solid.

where M_d, M_{Ce} and M_O represent the atomic weight of doping cations, cerium and oxygen, N_A is the Avogadro number and a_c is the lattice parameter calculated.

As shown in Fig. 4 the SEM micrograph of all LnSDC samples sintered at 1400 °C indicates that the surface has a good densification with very few residual pores and that average grain size is lower than 1.5 μm. This is consistent with the relative density values (Table 1) which are less than 100%. In Fig. 5, the grain size laser analysis carried out on the LaSDC powders proves that ultrasound vibrations during 20 min are necessary to dissociate the largest agglomerates. A monomodal particle distribution can also be seen, where the width of the size distribution (S) is between 1.9 and 2.9 μm (Table 1).

$$S = \frac{d_{90} - d_{10}}{d_{50}} \quad (5)$$

where d_{10}, d_{50} and d_{90} are the particle sizes when the accumulative distribution is 10%, 50% and 90% respectively. The powders have a severe agglomeration and broad size distribution.

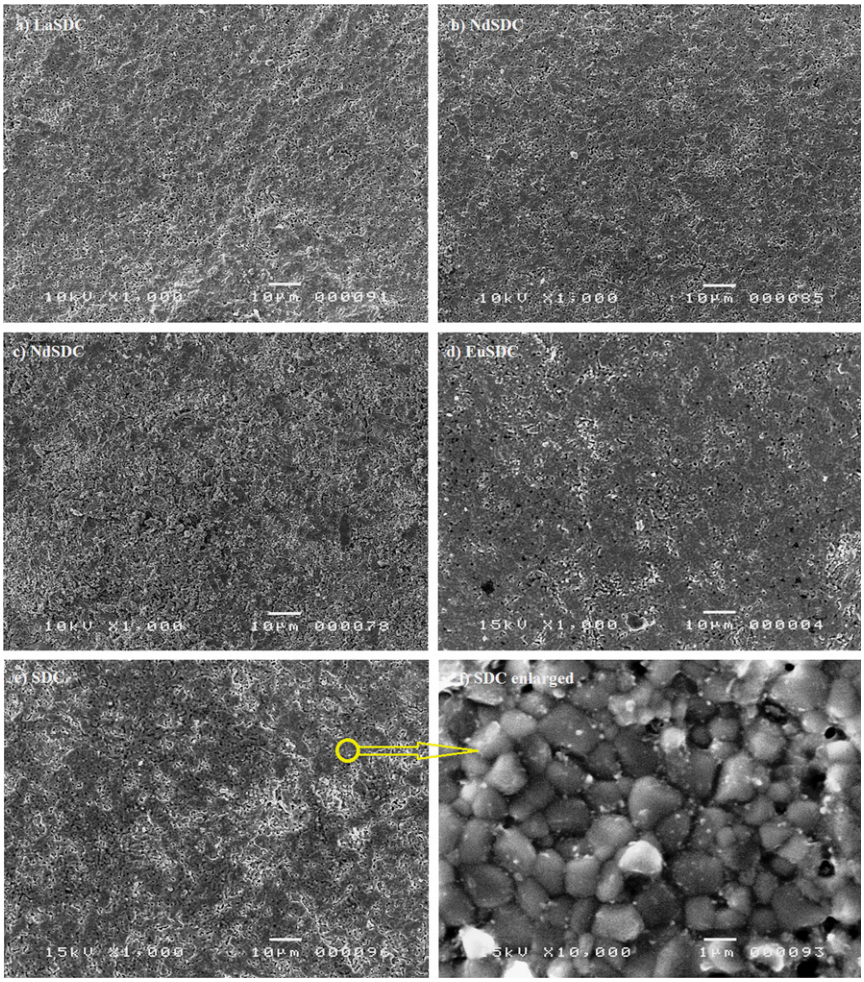

Fig. 4. SEM photographs of the sintered samples at 1400 °C for 5 h in air: (a) LaSDC, (b) NdSDC, (c) YSDC, (d) EuSDC, (e) SDC and (f) SDC enlarged.

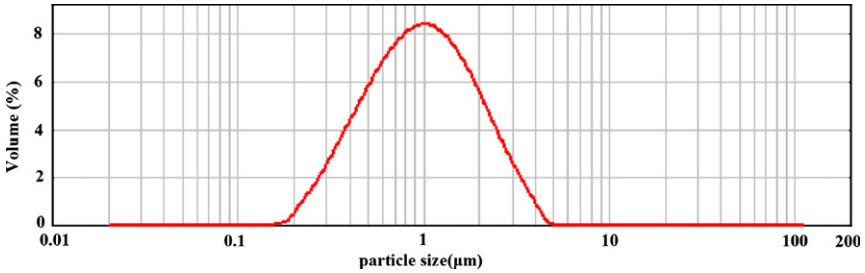

Fig. 5. Distribution of particles of $Ce_{0.8}Sm_{0.2}O_{1.9}$ ceramics by size.

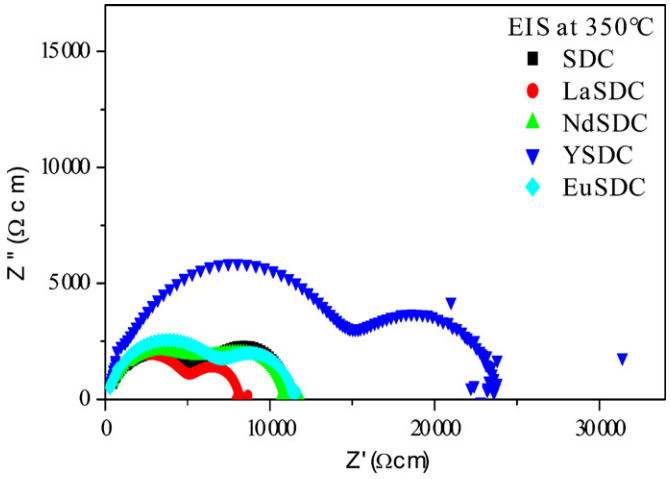

Fig. 6. Example of the impedance spectrum of an $Ag/Ce_{0.8}Sm_{0.1}Ln_{0.1}O_{1.9}/Ag$ cell at 400 °C.

3.4. Electrical characterization

Fig. 6 shows the Nyquist diagram obtained from pellets of LnSDC at 1400 °C. Those pellets were sintered at 1400 °C and had a relative density of 95%.

The impedance spectrum is composed of two contributions: the high frequency contribution (attributed to the response of the grains) and an intermediate frequency contribution (attributed to the grain boundaries). The various electrochemical contributions of material overlap require the refinement of the mathematical model by taking, once again, various parameters such as the resistance (R) and the constant phase element (CPE). To better describe the experimental Nyquist diagrams, a model series as shown in Fig. 7 was used for simplicity reasons. The contributions resulted in a series of R–CPE couples. In the equivalent circuit model, R_g is the grain interior resistance and R_{gb} is the grain boundary resistance. Depending on the temperature, the contributions are better or worse. The total resistance of the electrolyte is given by

$$R_t = R_g + R_{gb}$$

The conductivity can be obtained using the following equation:

$$\sigma = \frac{l}{S} \times \frac{1}{R} \tag{6}$$

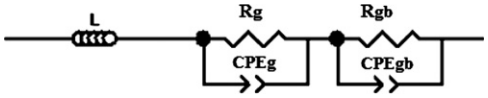

Fig. 7. Equivalent circuit used for fitting the impedance data.

where l is the thickness of the sample and S is the electrode surface area. The ratio l/S is the sample's geometric factor.

Activation energies (E_a), which are the sum of the association energy (E_{as}) and the migration energy (E_{mg}), were calculated by fitting the conductivity data to the Arrhenius relation for thermally activated conduction, given by

$$\sigma T = \sigma_0 \exp\left(-\frac{E_a}{kT}\right) = \sigma_0 \exp\left(-\frac{E_{as}+E_{mg}}{kT}\right) \tag{7}$$

where σ, T, k, E_a and σ_0 are the conductivity, absolute temperature, Boltzmann constant, activation energy and a pre-exponential factor, respectively.

Fig. 8(a)–(c) shows total, grain and grain boundary conductivity for the $Ce_{0.8}Sm_{0.1}Ln_{0.1}O_{1.9}$ (LnSDC) series. It shows that the behavior of all co-doped ceria is very similar to figures published by different authors [12–17]. A variation in the activation energy is observed as the radius of the dopant is changed, which is confirmed by Fu et al. [20] for doped ceria and Sibel Dikmen [12,13] for co-doped ceria.

As shown in Fig. 8(a) the Arrhenius plot of LnSDC ($Ln^{3+} = La^{3+}$, Nd^{3+}, Y^{3+}, Eu^{3+}), co-doping with the rare-earth cations mentioned above improved the total conductivity compared to SDC. Among the various co-doping cations, the La^{3+} gave the best results ($\sigma_{tot} = 6.59 \times 10^{-2}$ S cm^{-1} at 700 °C with $E_a = 0.85$ eV, see Table 2). These results proved that co-doping with samarium and the above-mentioned cations can further improve the electrical properties of ceria electrolytes.

Furthermore, a fracture in the Arrhenius plot for the LnSDC samples (Fig. 8(a)) can be observed, and it is comparable to results found in reports on doped [4,7,22] and co-doped ceria [14,19,23]. Fig. 8(a) also shows that significant bending occurs between 450 and 550 °C, which is interpreted as a transition from associated to disassociated behavior in defect clusters, and by consequence as a decrease in the activation energy [9,19]. Some authors have stated that the increase of activation energy may depend on the change of defects association from dimers to trimers

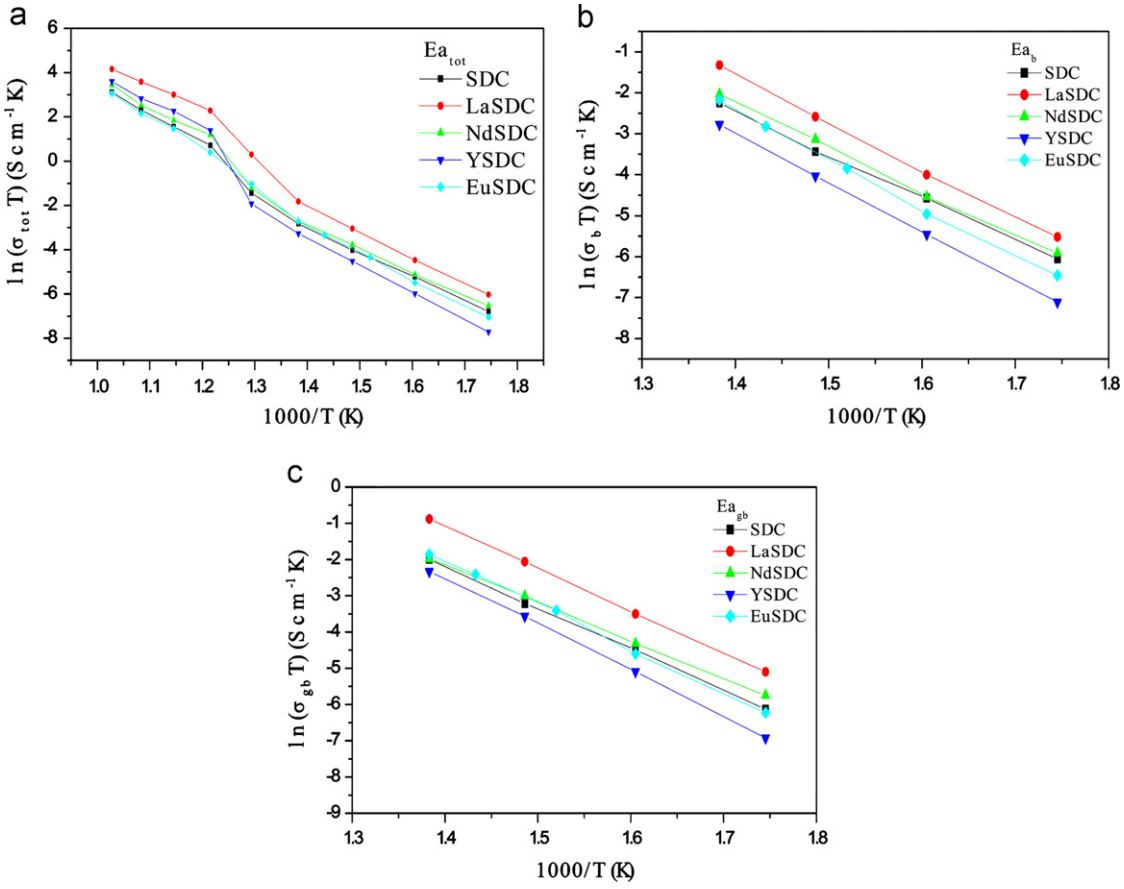

Fig. 8. Total (a), grain (b) and grain boundary (c) electrical conductivity obtained for $Ce_{0.8}Sm_{0.1}Ln_{0.1}O_{1.9}$ (Ln = La, Nd, Y, Eu) electrolyte sintered at 1400 °C.

Table 2
Activation energies and conductivity of $Ce_{0.8}Sm_{0.1}Ln_{0.1}O_{1.9}$ electrolytes.

Composition	Activation energy (eV)				Conductivity (10^{-2} S cm^{-1})
	E_g at 300–450 °C	E_{gb} at 300–450 °C	E_{tot} at 300–450 °C	550–700 °C	σ_{tot} at 700 °C
$Ce_{0.8}Sm_{0.2}O_{1.9}$	0.89	0.98	0.93	1.09	2.32
$Ce_{0.8}Sm_{0.1}La_{0.1}O_{1.9}$	0.99	1	1	0.85	6.59
$Ce_{0.8}Sm_{0.1}Nd_{0.1}O_{1.9}$	0.93	0.9	0.92	1.02	3.29
$Ce_{0.8}Sm_{0.1}Y_{0.1}O_{1.9}$	1.03	1.09	1.05	0.99	3.77
$Ce_{0.8}Sm_{0.1}Eu_{0.1}O_{1.9}$	1.02	1.05	1.03	1.20	2.2

and higher order clusters [14], in addition to the formation of microdomaines.

The pre-exponential factor, σ_0, as a function of the dopant ionic radius is shown in Fig. 9. The pre-exponential factor also varies with the nature of the dopant. However, the activation energy minimum and the electrical conductivity maximum are not necessarily associated with the same dopant nature, since the pre-exponential factor is also a function of the dopant's nature [24]. In general, for a particular dopant element, if the pre-exponential factor is increased, the activation energy would decrease [25]. But in the present case, the activation energy minimum and the electrical conductivity maximum are associated with the same dopant cation, i.e. the ionic conductivity increases with decreasing pre-exponential factor and is proportional to the activation energy. However, the interpretation of the phenomena involved in the conductivity of co-doped ceria with cations of different valence and size is complex [19], except for a decrease at a lower dopant concentration.

Table 1 shows that the grain boundary activation energies are consistently higher than the grain activation energies. Fig. 8(b and c) shows that the grain conductivity (σ_g) is lower than the grain boundary conductivity (σ_{gb}). The variation of activation energy and conductivity for the grain and grain boundary may therefore be due to the presence of attractive interactions between dopant cations and oxygen vacancies [19,25].

According to Li et al. [14] the differences in grain and grain boundary behavior for samples correspond to differences in the trivalent dopant segregation. Many factors

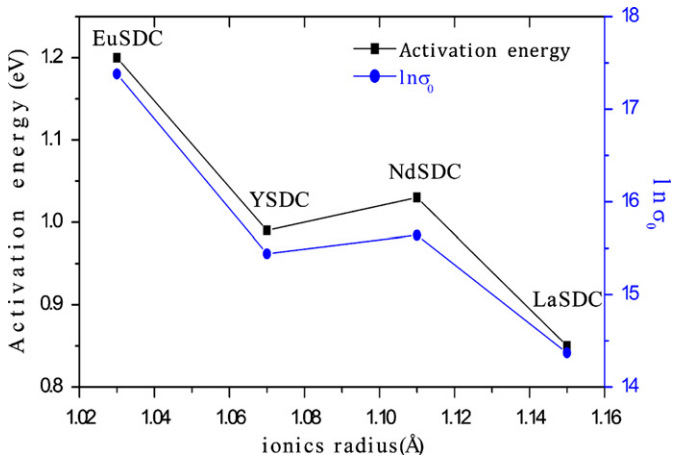

Fig. 9. Variation of activation energy and pre-exponential factor as a function of dopant cation radius in $Ce_{0.8}Sm_{0.1}Ln_{0.1}O_{1.9}$.

may affect the segregation of trivalent additives, including differences in powder preparation methods, sintering temperature and the corresponding differences in grain size. Furthermore, the level of contamination by impurities (silica) is also known to affect the grain boundary behavior. These issues will be dealt with in future work.

4. Conclusions

The single-phase fluorites $Ce_{0.8}Sm_{0.1}Ln_{0.1}O_{1.9}$ were prepared by the citric acid–nitrate process. The results revealed that sintering pellet $Ce_{0.8}Sm_{0.1}La_{0.1}O_{1.9}$ at 1400 °C for 5 h exhibits the highest ionic conductivity with the lowest activation energy (6.59×10^{-2} S cm^{-1}, 0.85 eV). The conductivity of LnSDC samples at 700 °C was as follows: LaSDC > YSDC > NdSDC > SDC > EuSDC. The activation energy of LnSDC in the temperature range between 550 °C and 700 °C was ranked as follows: EuSDC > SDC > NdSDC > YSDC > LaSDC. These co-doped ceria materials can be used as electrolyte material for IT-SOFC applications.

Acknowledgment

This work was supported by the Ministry of Higher Education and Scientific Research of Tunisia. The author would also like to thank the language expert Nayua Abdelkefi for proofreading the manuscript.

References

[1] H. Yahiro, Y. Eguchi, K. Eguchi, H. Arai, Oxygen ion conductivity of the ceria–samarium oxide system with fluorite, Journal of Applied Electrochemistry 18 (1988) 527.
[2] T. Karaca, T.G. Altıncekic, M.F. Oksuzomer, Synthesis of nanocrystalline samarium-doped CeO_2 (SDC) powders as a solid electrolyte by using a simple solvothermal route, Ceramics International 36 (2010) 1101–1107.
[3] D.J. Seo, K.O. Ryu, S.B. Park, K.Y. Kim, R.H. Song, Synthesis and properties of $Ce_{1-x}Gd_xO_{2-x/2}$ solid solution prepared by flame spray pyrolysis, Materials Research Bulletin 41 (2006) 359–366.
[4] I.E.L. Stephens, J.A. Kilner, Ionic conductivity of $Ce_{1-x}Nd_xO_{2-x/2}$, Solid State Ionics 177 (2006) 669–676.
[5] S. Dikmen, P. Shuk, M. Greenblatt, Hydrothermal synthesis and properties of $Ce_{1-x}Bi_xO_{2-\delta}$ solid solutions, Solid State Ionics 112 (1998) 299–307.
[6] C. Peng, Y.N. Liu, Y.X. Zheng, Nitrate–citrate combustion synthesis and properties of $Ce_{1-x}Ca_xO_{2-x}$ solid solutions, Materials Chemistry and Physics 82 (2003) 509–514.
[7] C. Peng, Z. Zhang, Nitrate–citrate combustion synthesis of $Ce_{1-x}Gd_xO_{2-x/2}$ powder and its characterization, Ceramics International 33 (2007) 1133–1136.
[8] Y.P. Fu, S.H. Chen, Preparation and characterization of neodymium-doped ceria electrolyte materials for solid oxide fuel cells, Ceramics International 36 (2010) 483–490.
[9] M. Mogensen, N.M. Sammes, G.A. Tompsett, Physical, chemical and electrochemical properties of pure and doped ceria, Solid State Ionics 129 (2000) 63–94.
[10] B.C.H. Steele, Appraisal of $Ce_{1-y}Gd_yO_{2-y/2}$ electrolytes for IT-SOFC operation at 500 °C, Solid State Ionics 129 (2000) 95–110.
[11] S.R. Hui, J. Roller, S. Yick, X. Zhang, C. Decès-Petit, Y. Xie, R. Maric, D. Ghosh, A brief review of the ionic conductivity enhancement for selected oxide electrolytes, Journal of Power Sources 172 (2007) 493–502.
[12] S. Dikmen, Effect of co-doping with Sm^{3+}, Bi^{3+}, La^{3+}, and Nd^{3+} on the electrochemical properties of hydrothermally prepared gadolinium-doped ceria ceramics, Journal of Alloys and Compounds 491 (2010) 106–112.
[13] S. Dikmen, H. Aslanbay, E. Dikmen, O. Şahin, Hydrothermal preparation and electrochemical properties of Gd^{3+} and Bi^{3+}, Sm^{3+}, La^{3+}, and Nd^{3+} co-doped ceria-based electrolytes for intermediate temperature-solid oxide fuel cell, Journal of Power Sources 195 (2010) 2488–2495.
[14] B. Li, Y. Liu, X. Wei, W. Pan, Electrical properties of ceria Co-doped with Sm^{3+} and Nd^{3}, Journal of Power Sources 195 (2010) 969–976.
[15] H.-C. Yao, Y.-X. Zhang, J.-J. Liu, Y.-L. Li, J.-S. Wang, Z.-J. Li, Synthesis and characterization of Gd^{3+} and Nd^{3+} co-doped ceria by using citric acid–nitrate combustion method, Materials Research Bulletin 46 (2011) 75–80.
[16] L. Gao, M. Zhou, Y. Zheng, H. Gu, H. Chen, L. Guo, Effect of zinc oxide on yttria doped ceria, Journal of Power Sources 195 (2010) 3130–3134.
[17] Y. Zheng, L. Wu, H. Gu, L. Gao, H. Chen, L. Guo., The effect of Sr on the properties of Y-doped ceria electrolyte for IT-SOFCs, Journal of Alloys and Compounds 486 (2009) 586–589.
[18] V.P. Kumar, Y.S. Reddy, P. Kistaiah, G. Prasad, C.V. Reddy., Thermal and electrical properties of rare-earth co-doped ceria ceramics, Materials Chemistry and Physics 112 (2008) 711–718.
[19] S. Ramesh, V.P. Kumar, P. Kistaiah, C.V. Reddy, Preparation, characterization and thermo electrical properties of co-doped $Ce_{0.8-x}Sm_{0.2}Ca_xO_{2-\delta}$ materials, Solid State Ionics 181 (2010) 86–91.
[20] Y.P. Fu, S.H. Chen, J.J. Huang, International Journal of Hydrogen Energy 35 (2010) 745–752.
[21] S. Sameshima, T. Ichikawa, M. Kawaminami, Y. Hirata., Thermal and mechanical properties of rare earth-doped ceria ceramics, Materials Chemistry and Physics 61 (1999) 31–35.
[22] D.P. Coll, D.M. Lopez, P. Nunez, S. Pinol, J.R. Frade, Grain boundary conductivity of $Ce_{0.8}Ln_{0.2}O_{2-\delta}$ ceramics (Ln=Y, La, Gd, Sm) with and without Co-doping, Electrochimica Acta 51 (2006) 6463–6469.
[23] X. Sha, Z. Lu, X.Q. Huang, J. Miao, L. Jia, X.sh. Xin, W. Su, Preparation and properties of rare earth co-doped $Ce_{0.8}Sm_{0.2-x}Y_xO_{1.9}$ electrolyte materials for SOFC, Journal of Alloys and Compounds 424 (2006) 315–321.
[24] I.E.L. Stephens, J.A. Kilner, Ionic conductivity of $Ce_{1-x}Nd_xO_{2-x/2}$, Solid State Ionics 177 (2006) 669–676.
[25] S. Omar, E.D. Wachsman, J.C. Nino, Higher conductivity Sm^{3+} and Nd^{3+} co-doped ceria-based electrolyte materials, Solid State Ionics 178 (2008) 1890.